Nanoscale

PAPER

View Article Online
View Journal | View Issue

Cite this: *Nanoscale*, 2025, **17**, 2878

Published on 06 January 2025. Downloaded by SUSTech on 2/2/2025 12:20:35 PM.

The effect of atomic vibration on thermal transport in diatomic semiconductors investigated *via ab initio* molecular dynamics†

Dian Huang,[a] Guihua Tang, *[a] Zhibin Gao [b] and Shengying Yue*[c]

Received 12th December 2024,
Accepted 4th January 2025

DOI: 10.1039/d4nr05240d

rsc.li/nanoscale

Based on the *ab initio* molecular dynamics (AIMD), the temperature and velocity statistics of diatomic semiconductors were proposed to be classified by atomic species. The phase differences resulting from lattice vibrations of different atoms indicated the presence of anharmonicity at finite atomic temperatures. To further explore the electronic properties, the effect of temperature on electrostatic potential field vibrations in semiconductors was studied, and the concept of electrostatic potential oscillation (EPO) at finite atomic temperature was introduced. It was confirmed that EPO in semiconductors was driven by lattice vibrations at finite temperatures. As the temperature increased, both the intensity of EPO and the rate of EPO change in heavy and light atoms increased, influencing electron thermal transport. To characterize the uncertainties in atomic lattice vibrations and EPO, the entropies of atomic EPO, atomic velocity of EPO (VEPO), atomic temperature, and atomic velocity were defined, with results consistent with the principle of entropy increase. This study not only aids in understanding the fundamental physical picture of electronic properties in semiconductors at finite temperatures but also provides a method for describing their uncertainties. The new theoretical concepts and statistical methods presented here can advance the understanding of electron thermal transport issues in semiconductor devices.

1. Introduction

The ongoing advancements in miniaturization and high power density of electronic devices have made them increasingly susceptible to temperature fluctuations during operation.[1,2] Considerable research has focused on controlling junction temperature fluctuations in electronics. It is widely believed that prolonged junction temperature fluctuations within a device can induce thermal stresses between neighboring stacked material layers,[3,4] which can ultimately degrade the performance of the device. In applications, such as electronic chips and thermoelectric cooling devices, precise temperature control[5–7] faces significant challenges due to stringent thermal management and stability requirements. Nevertheless, it remains crucial for ensuring the reliability and longevity of electronic devices. Macroscopic temperature indicates the degree of heat (hotness or coldness) in electronics, while microscopic temperature reflects the intensity of thermal motion of microscopic particles in the constituent materials of electronics. Atoms in solids consist of ion cores and valence electrons.[8] As the temperature of atoms in a solid changes, it induces lattice vibrations and alters the distribution of electrons. These changes affect the interactions among heat carriers, consequently impacting the thermal conductivity of the solid.[9,10]

The third-generation semiconductors, including gallium nitride (GaN), 4H-silicon carbide (4H-SiC, referred to as SiC in this work), zinc oxide (ZnO), and aluminum nitride (AlN), are wide-bandgap semiconductors with a bandgap value E_g > 2.3 eV.[11,12] They are currently the most promising and widely used materials in semiconductor chip development, integrated circuits, aerospace, and other fields due to their outstanding thermal conductivity, high electron mobility, and high breakdown voltage. InN is a narrow-bandgap semiconductor, widely used in ultra-high-speed electronic devices.[13] Previous research has primarily focused on the lattice thermal conductivity of semiconductors, where temperature changes affect the distribution of the electric field around atoms, often overlooking the role of electrons. The mechanism of electron transport in semiconductors is not fully understood. It is known that

[a]MOE Key Laboratory of Thermo-Fluid Science and Engineering, School of Energy and Power Engineering, Xi'an Jiaotong University, Xi'an 710049, China. E-mail: ghtang@mail.xjtu.edu.cn
[b]State Key Laboratory for Mechanical Behavior of Materials, School of Materials Science and Engineering, Xi'an Jiaotong University, Xi'an 710049, China
[c]Laboratory for Multiscale Mechanics and Medical Science, SV LAB, School of Aerospace, Xi'an Jiaotong University, Xi'an 710049, China. E-mail: syyue@xjtu.edu.cn

†Electronic supplementary information (ESI) available. See DOI: **https://doi.org/10.1039/d4nr05240d**

This journal is © The Royal Society of Chemistry 2025

Published on 06 January 2025. Downloaded by SUSTech on 2/2/2025 12:20:35 PM.

lattice vibrations (vibration of ion cores) can cause electrostatic potential oscillation (EPO). To study heat transfer by electrons, the EPO model to assess the electronic thermal conductivity (κ_e) of metals was proposed.[14] Compared to the BTE method, the electronic thermal transport in metals can be better described without explicitly exploring specific scattering processes. The EPO model has also been applied to predict the electronic thermal transport of ε-iron under Earth's core conditions, successfully addressing complex geophysical problems in extreme environments.[15] Nevertheless, it is essential to clarify the relationship between different atoms and EPO in semiconductors, and the mechanisms by which temperature drives the generation of EPO around these atoms. It is crucial to understand the impact of temperature on electron transport.

As temperature changes, the degree of lattice vibrations and EPO change accordingly. Entropy has been used to microscopically describe the degree of uncertainty within systems[16–18] and it has important applications in multiple areas, including physics, chemistry, information theory, and ecology. In the study of temperature-driven EPO, an increase in temperature intensifies lattice vibrations and electron movements, thereby enhancing the uncertainty associated with both lattice vibrations and electron movements. The definition of Shannon entropy, combined with the *ab initio* method, quantitatively characterizes the uncertainty of parameters such as EPO and atomic temperature. It establishes a basis for understanding the uncertainty of heat transfer by electrons in semiconductors.

In this work, firstly, a method for statistically analyzing temperatures based on atomic species is proposed, offering a new approach for an in-depth understanding of heat transfer between different atoms. The temperature fluctuations of heavy and light atoms in AlN, GaN, InN, SiC, and ZnO were calculated at four temperatures (100, 300, 500, and 700 K) according to the atomic species. Secondly, the relationship between lattice vibrations and EPO of heavy and light atoms was confirmed at different temperatures, graphically describing the EPO and the velocity of EPO. The temperature effects on EPO in semiconductors were studied. Finally, the EPO entropy, velocity of EPO entropy, atomic velocity entropy, and atomic temperature entropy are defined and discussed.

2. Computational methods

Based on the *ab initio* molecular dynamics (AIMD), the projector augmented-wave (PAW) method[19,20] was implemented using the Vienna *ab initio* simulation package (VASP),[21,22] and the Perdew, Burke, and Ernzerhof (PBE) generalization under the generalized gradient approximation[23] (GGA) to describe the exchange–correlation functional.[24] The VASP code was modified to extract the instantaneous velocities of the atoms. The cut-off energy was chosen as the default value of the pseudopotential file, the Brillouin zone sampling was chosen as Γ point only, and the temperature control was performed by using the Nosé–Hoover method.[25] The AIMD simulation was carried out in the canonical ensemble (constant numbers of particles, volume, and temperature), with a time step of 1 fs. The total simulation time for the AIMD was 100 ps. The Brillouin zone was sampled using a Γ-centered Monkhorst–Pack 6 × 3 × 2 *k*-point grid, and the total energy (convergence of forces) was less than 10^{-6} eV (0.01 eV Å^{-1}) in the calculation of the total density of states (TDOS). Post-processing was performed with the VASPKIT code.[26]

The thermal conductivity at temperature T can be obtained using eqn (1).

$$\kappa^{\alpha\beta} = \frac{1}{k_B T^2 N V} \sum_{\lambda} f_{\lambda}^{0}(1 + f_{\lambda}^{0})(\hbar\omega_{\lambda})^2 v_{\lambda}^{\alpha} F_{\lambda}^{\beta} \tag{1}$$

where k_B is the Boltzmann constant, N is the total number of Brillouin zone grid points, V is the volume of the unit cell, ω_λ is the phonon angular frequency, f_λ^0 is the Bose–Einstein distribution function, v_λ is the group velocity, F_λ is the phonon mean free displacement, $\hbar$ is the Planck constant, and λ includes the phonon branch index and wave vector.

The Grüneisen parameter can be calculated using eqn (2).

$$\gamma = -\frac{V}{\omega_i}\frac{\partial \omega_i}{\partial V} \tag{2}$$

where V represents the volume and ω_i represents the frequency.

By addressing the Schrödinger equation for a multiparticle system, the average electrostatic potential ($\overline{V_n}$) of each ion core is obtained, as in eqn (3).

$$\overline{V_n} = \int V(r)\rho_{\text{test}}(|r - R_n|)\mathrm{d}^3 r \tag{3}$$

where r denotes the position of the electron, ρ_{test} denotes a test charge with the norm 1, R_n denotes the position of the ion cores, and $V(r)$ denotes the potential function.

The power spectral density (PSD) method is a commonly used tool for analyzing random vibrations. A real smooth random process is established, and its Fourier transform is defined as its power spectral density, as shown in eqn (4). The inverse Fourier transform of $S(f)$ is the original signal and the autocorrelation function of $s(t)$ is in eqn (5). Where $E[\cdot]$ denotes the average or mathematic expectation of $[\cdot]$.

$$S(f) = \int_{-\infty}^{+\infty} s(t)e^{-j2\pi ft}\mathrm{d}t \tag{4}$$

$$s(t) = E[\zeta(\tau)\zeta(\tau + t)] \tag{5}$$

A 600 eV plane-wave cutoff energy and a total energy of less than 10^{-8} eV were used for κ_e and phonon thermal conductivity (κ_{ph}). The unit cell κ_e in GaN was calculated using the AMSET software[27] with a 45 × 45 × 25 *k*-point grid. The elastic constants, dielectric constants deformation potential and κ_{ph} were gained with a 7 × 7 × 4 *k*-point grid. When calculating κ_{ph}, 2 × 2 × 2 supercells of GaN and InN were constructed, and the second-order force constants were performed with phonopy.[28] The third-order force constants were obtained using the thir-

Published on 06 January 2025. Downloaded by SUSTech on 2/2/2025 12:20:35 PM.

dorder package.[29] According to the second-order, and third-order force constants and convergence testing in the ESI,† the cutoff radius was set to the 12th nearest neighbor. The phonon thermal conductivities were calculated using the ShengBTE[29] package, with the q-mesh settings for GaN and InN were set to 9 × 9 × 9 and 11 × 11 × 11, respectively.

3. Results and discussion

3.1 Thermodynamic stability of semiconductors

The relative atomic masses of Al, N, Ga, In, Si, C, Zn, and O are 26.98, 14.00, 69.72, 114.81, 28.08, 12.01, 65.38, and 15.99, respectively. Thus, the heavy (light) atoms in the AlN, GaN, InN, ZnO, and SiC systems are Al (N), Ga (N), In (N), Zn (O), and Si (C), respectively. In the study of statistical temperature fluctuations by atomic species, the AIMD models, as shown in Fig. 1a and b for AlN, GaN, InN, and ZnO, are constructed using the 2 × 4 × 4 supercells containing a total of 128 atoms and these models belong to the $P6_3mc$ space group. To maintain a consistent total number of atoms, a model for SiC was also constructed with the same total number of atoms while ensuring that the space group ($P6_3mc$) remains constant. The unit cell lattice constants of AlN, GaN, InN, ZnO, and SiC are a = 3.12 Å, c = 5.01 Å; a = 3.22 Å, c = 5.24 Å; a = 3.55 Å, c = 5.73 Å; a = 3.28 Å, c = 5.30 Å; and a = 3.09 Å, c = 10.12 Å, respectively. These values are in good agreement with the results from previous studies.[30–33] The spacing between the two layers of atoms in AlN, GaN, ZnO, SiC and InN are 5.01, 5.24, 5.30, 5.06, 5.73 Å, respectively.

The thermodynamic stability of AlN, GaN, InN, ZnO, and SiC at 100, 300, 500, and 700 K was tested based on AIMD simulations, as shown in Fig. 1c and d and Fig. S1.† The free energy fluctuations of AlN, GaN, InN, ZnO, and SiC after 1 ps of simulation at four different temperatures are small, with all systems vibrating near their equilibrium positions. Additionally, the temperature fluctuations are close to the initial temperatures, indicating that AlN, GaN, InN, ZnO, and SiC are thermodynamically stable at 100, 300, 500, and 700 K.

3.2 Temperature statistics by atomic species

The temperatures of the constituent atoms in semiconductors were calculated separately based on the average translational kinetic energy of gas molecular thermal motion as in eqn (6) and (7).

$$\bar{\varepsilon} = \frac{3Nk_{\mathrm{B}}T}{2} = \frac{1}{2}\sum_{\mathrm{i}=1}^{N} m_{\mathrm{i}}v_{\mathrm{i}}^{2} \tag{6}$$

$$v_{\mathrm{i}}^{2} = v_{x}^{2} + v_{y}^{2} + v_{z}^{2} \tag{7}$$

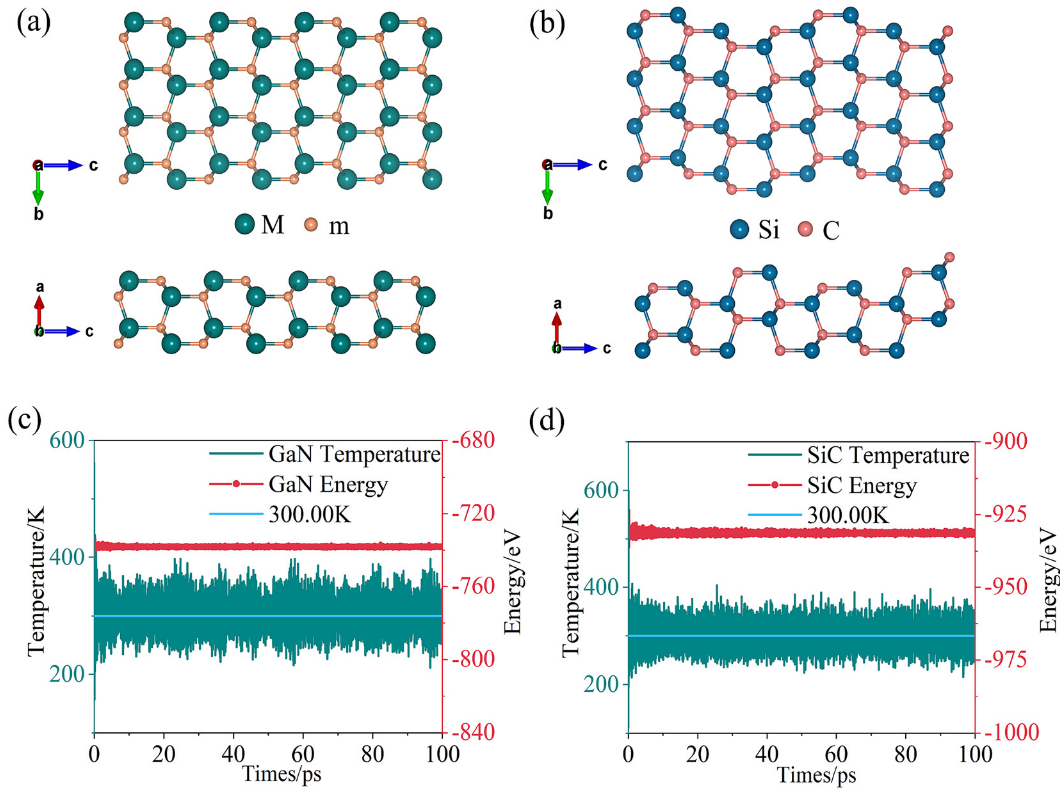

Fig. 1 Top and side views of the AIMD initial models for (a) AlN, GaN, InN, and ZnO (where M and m represent Al and N, Ga and N, In and N, and Zn and O, respectively) and (b) SiC. Different colors distinguish the various constituent atoms. Temperature fluctuations and total energy fluctuations of (c) GaN and (d) SiC over 100 ps at 300 K.

This journal is © The Royal Society of Chemistry 2025

Published on 06 January 2025. Downloaded by SUSTech on 2/2/2025 12:20:35 PM.

Fig. 2 (a) Schematic of the temperature statistics of atoms by atomic species in diatomic semiconductors. Temperature fluctuations of (b) Al and N in AlN, (c) Zn and O in ZnO, (d) Si and C in SiC, (e) Ga and N in GaN, and (f) In and N in InN between 20 and 100 ps at 300 K (average temperatures of atoms are labeled).

where N is the number of gas molecules, T is the temperature, m_i and v_i are the mass and velocity of the gas molecules, respectively. v_x, v_y and v_z represent the components of the velocity in the x, y, z direction, respectively.

When a heat source is introduced into a diatomic semiconductor, the temperatures of the heavy and light atoms are analyzed separately according to the masses of their constituent atoms shown in Fig. 2a. The temperature fluctuations of heavy and light atoms in the five materials at 100, 300, 500, and 700 K are calculated based on eqn (8).

$$T_M = \frac{\sum_i M_i {v_i}^2}{3Nk_B}, \quad T_m = \frac{\sum_j m_j {v_j}^2}{3Nk_B} \tag{8}$$

where T_M and T_m are the temperatures, M_i and m_j are the masses, and v_i and v_j are the velocities of heavy and light atoms, respectively.

Firstly, when AlN, ZnO and SiC are at 300 K, the average temperatures of heavy and light atoms in AlN, SiC, and ZnO are approximately equal in Fig. 2b–d, *i.e.*, $T_{Al} = T_N$, $T_{Zn} = T_O$, $T_{Si} = T_C$. However, when GaN and InN are at 300 K, the average temperatures of Ga and N, In and N are not equal in Fig. 2e and f, *i.e.*, $T_{Ga} \neq T_N$, $T_{In} \neq T_N$. Similar results can be found for other temperatures in AlN, GaN, SiC, ZnO and InN, as shown in Fig. S2.† It is due to the competitive mechanism between the square of the velocity ratio and the mass ratio of heavy to light atoms. When diatomic semiconductors are in thermal equilibrium, the temperatures of heavy and light atoms at the same statistical time exhibit three possible outcomes: the temperatures of both are approximately equal, and the heavy

Published on 06 January 2025. Downloaded by SUSTech on 2/2/2025 12:20:35 PM.

atom temperature is greater than (or less than) the light atom temperature.

Secondly, to maintain thermal equilibrium in diatomic semiconductors, the temperature changes in heavy and light atoms have opposite trends at adjacent moments. When the temperature of the heavy atoms rises, the temperature of the light atoms decreases at adjacent moments. Temperature fluctuations lead to the excitation of valence electrons, which interact with lattice vibrations of heavy and light atoms, subsequently causing heat transfer.

Finally, the average translational kinetic energy of the thermal motion of molecules is proportional to the temperature. The average velocities of Al and N, Ga and N, Zn and O, Si and C, and In and N between 20 and 100 ps at 100, 300, 500, and 700 K were calculated as shown in Table 1. It can be concluded that the average velocity of light atoms is greater than that of heavy atoms, regardless of system temperature. In thermal equilibrium, the velocities of molecules follow the Maxwell–Boltzmann distribution, resulting in lighter atoms, which have a smaller mass compared to heavier atoms, moving at higher speeds. As the temperature rises, the atomic vibrations intensify and their velocities increase. The essence of the temperature and velocity fluctuation changes of heavy and light atoms in a diatomic semiconductor at the same temperature is its interaction with electrons, which produces heat transfer and kinetic energy exchange.

Table 1 The average velocities (m s^{-1}) of Al and N, Ga and N, Zn and O, Si and C, and In and N calculated between 20 and 100 ps at 100, 300, 500, and 700 K. The ratio denotes the average velocity of heavy atoms to the average velocity of light atoms

	100 K	300 K	500 K	700 K
v_{Al}/v_N	2484/3275	4192/5832	5382/7570	6415/8893
v_{Ga}/v_N	1139/4020	2386/6281	3199/7876	3871/9144
v_{Zn}/v_O	1522/3208	2676/5480	3456/7071	4125/8295
v_{Si}/v_C	2407/3582	4135/6260	5296/8147	6302/9584
v_{In}/v_N	787/4186	1291/7352	2179/8588	2774/9746

3.3 Anharmonicity of lattice vibrations at a finite temperature

To demonstrate the existence of anharmonicity in lattice vibrations of atoms in semiconductors at finite temperatures, the temperature variation curves of Al and N, Ga and N, and In and N atoms at 300 K are selected, as shown in Fig. 3a–c. It can be observed that there are different phase differences ($\Delta\varphi_1$, $\Delta\varphi_2$) in the temperature fluctuations of Al and N, Ga and N, and In and N atoms. It is widely recognized that temperature fluctuations cause vibrations of ion cores (lattice vibrations) in diatomic semiconductors. Therefore, the lattice vibrations of Al and N, Ga and N, and In and N exhibit different phase differences, which leads to the existence of anharmonicity in the atomic vibrations of AlN, GaN, and InN at 300 K.

The anharmonicity of GaN and InN are compared. The optimized lattice constants for GaN are a = 3.22 Å, c = 5.24 Å, and those for InN are a = 3.58 Å, c = 5.79 Å. The phonon spectra of GaN and InN at 300 K demonstrate the dynamical stability of both materials, featuring 3 acoustic phonon branches and 9 optical phonon branches, as shown in Fig. 3d. The difference in atomic mass leads to a bandgap between phonon branches.

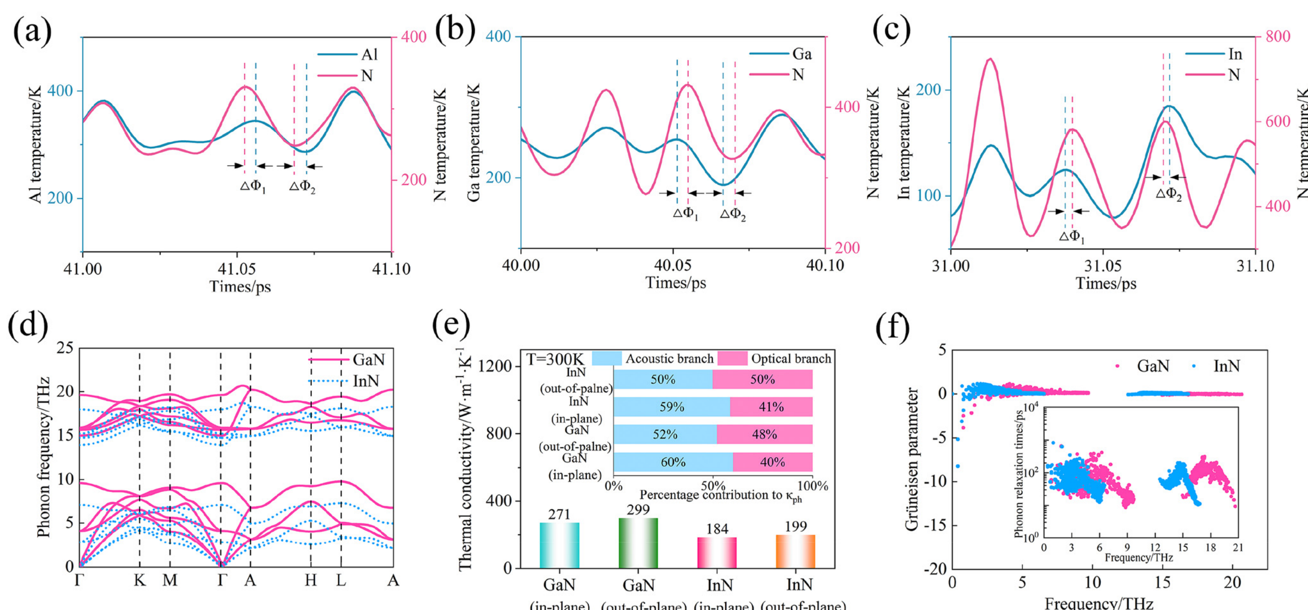

Fig. 3 Temperature fluctuation curves of (a) Al and N, (b) Ga and N, and (c) In and N in AlN, GaN, and InN at 300 K, with phase differences marked. (d) Phonon dispersions of GaN and InN at 300 K. (e) Phonon thermal conductivities of GaN and InN at 300 K. The embedded figure shows the contributions of acoustic and optical phonon branches to the thermal conductivity. (f) Grüneisen parameter of GaN and InN. The embedded figure shows the phonon relaxation times of GaN and InN at 300 K.

This journal is © The Royal Society of Chemistry 2025

Published on 06 January 2025. Downloaded by SUSTech on 2/2/2025 12:20:35 PM.

The phonon spectrum of InN shifts overall toward lower frequencies compared to that of GaN, accompanied by the softening of phonon branches, which will result in a decrease in phonon group velocity and an increase in phonon anharmonicity. The κ_{ph} of GaN at 300 K was calculated, as shown in Fig. 3e, with the in-plane thermal conductivity as 271 W m^{-1} K^{-1} and the out-of-plane thermal conductivity as 299 W m^{-1} K^{-1}, which is close to the results from previous work.[31,34] For InN, the κ_{ph} has the in-plane thermal conductivity as 184 W m^{-1} K^{-1} and the out-of-plane thermal conductivity as 199 W m^{-1} K^{-1}. Overall, the κ_{ph} of InN is lower than that of GaN. The in-plane thermal conductivity of GaN and InN is contributed by low-frequency acoustic phonons, accounting for 60% and 59%, respectively, while the optical phonons contribute 40% and 41%. This indicates that the κ_{ph} is primarily derived from low-frequency acoustic phonons. In contrast, their out-of-plane thermal conductivity is nearly equally contributed by acoustic and optical phonons, each accounting for approximately 50%.

In general, a larger Grüneisen parameter indicates stronger anharmonicity in the material system. The Grüneisen parameter of InN has a broader distribution compared to that of GaN, suggesting that InN exhibits greater anharmonicity, as shown in Fig. 3f. Comparing the scattering relaxation times of GaN and InN, the scattering relaxation time of InN shifts toward the low-frequency phonon region, where scattering is more concentrated. Since the κ_{ph} is primarily contributed by phonons in the low-frequency region, the κ_{ph} of InN is lower than that of GaN.

The PSD method is used to convert the velocity signals of ion cores in AlN, GaN, and InN into the vibrational density of states. As the atomic mass differences increase from AlN to GaN and then to InN, the bandgap in the VDOS also increases, as shown in Fig. 4a. In the VDOS of AlN, contributions below the bandgap (12.3–14 THz) are mainly from Al, while contributions above the bandgap are from a combination of Al and N. In the VDOS of GaN, contributions below the bandgap (10.3–13.0 THz) are mainly from Ga, and contributions above the bandgap are from N atoms. In the VDOS of InN, contributions below the bandgap (6.7–10.9 THz) are primarily from In, while those above the bandgap are from N atoms. The distribution of atomic contributions is consistent with that from the previous study.[35]

The total density of states (TDOS) of GaN under 300 K at 40, 80, and 100 ps was calculated, as shown in Fig. 4b. Band engineering[36,37] has been employed to manipulate the electronic properties of semiconductors. Due to temperature fluctuations occurring in GaN at a controlled temperature of 300 K, the energy band gap between the valence band maximum and conduction band minimum is also influenced by these thermal effects. The bandgap values are 1.61 eV at 40 ps, 1.63 eV at 80 ps, and 1.56 eV at 100 ps. Consequently, temperature fluctuations further alter the thermal transport properties of electrons in GaN.

3.4 EPO of semiconductors at a finite atomic temperature

In semiconductors, electrons move due to thermal excitation, creating an electric field. It will assist in understanding electron transport in semiconductors by investigating the magnitude of the electrostatic potential (EP) field around heavy and light atoms in diatomic semiconductors, the relationship between EPO and lattice vibrations, and the impact of temperature on driving oscillations of the EP field.

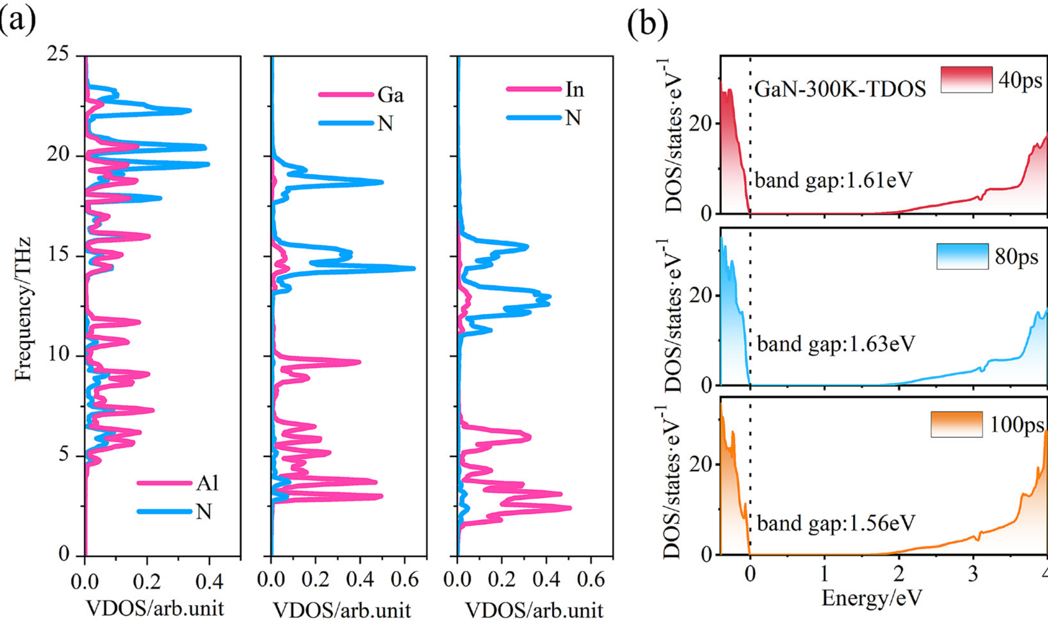

Fig. 4 (a) Vibrational density of states (VDOS) of Al and N, Ga and N, and In and N. (b) TDOS diagram of GaN at 300 K for 40, 80, and 100 ps (the dashed line represents the Fermi energy level).

View Article Online

Published on 06 January 2025. Downloaded by SUSTech on 2/2/2025 12:20:35 PM.

According to eqn (3), it can be noted that lattice vibrations (vibration of ion cores) can lead to spatial EPO. To verify that the EPO in the diatomic semiconductor is induced by lattice vibrations and to explore the relationship between the velocity of EPO and the velocity of lattice vibrations, similar to temperature statistics by atomic species, AIMD models for GaN were constructed using supercells with a total atomic number of 32.

The relationship between lattice vibrations and EPO is described using the PSD method. Four signals of $D_{\text{ion}}(t)$, $V_{\text{ion}}(t)$, $U_{\text{ion}}(t)$ and $\Delta U_{\text{ion}}(t)$ are considered, which represent the displacement, velocity, displacement of electrostatic potential (DEP), and VEPO of the ion cores, respectively.

(1) The displacement of the ion cores $D_{\text{ion}}(t)$. The change in the position of the ion cores is considered in the PSD analysis to obtain the spectral density of atomic displacement (S_D), which reflects the ion core vibrations in real space.

(2) Velocity of the ion cores $V_{\text{ion}}(t)$. The VASP code was modified to output the instantaneous velocity of the ion cores at each time step, and the PSD analysis was applied to obtain the spectral density of atomic velocity (S_V), which is the probability density function that describes the velocity vibrations of ion cores.

(3) The electrostatic potential (EP) displacement of the ion cores $U_{\text{ion}}(t)$. The PSD technique was applied to transform the

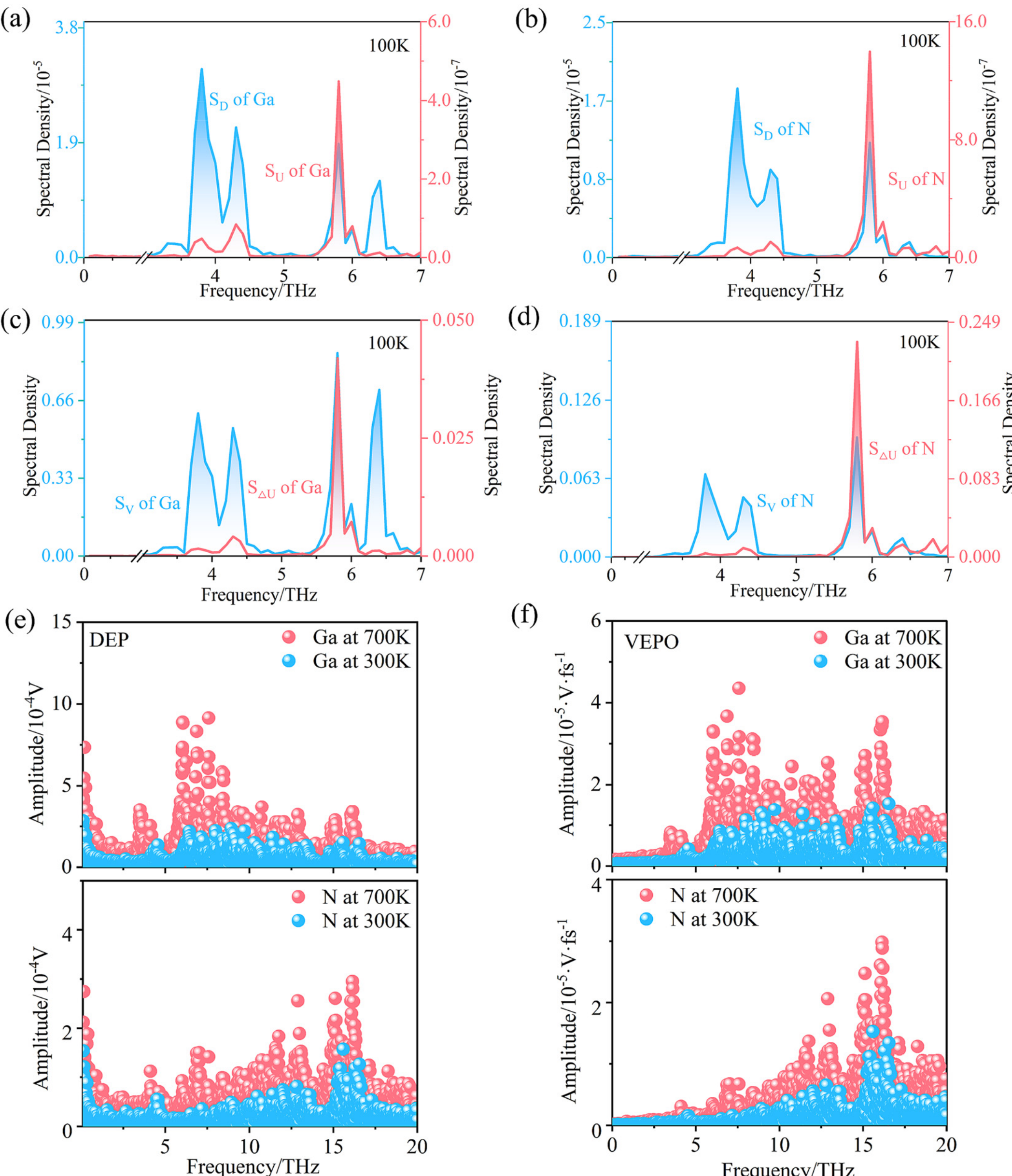

Fig. 5 S_D and S_U of (a) Ga and (b) N atoms, S_V and $S_{\Delta U}$ of (c) Ga and (d) N atoms in GaN at 100 K. FFT amplitudes of (e) DEP and (f) VEPO of ion cores in Ga and N atoms at 300 and 700 K in GaN.

This journal is © The Royal Society of Chemistry 2025

Published on 06 January 2025. Downloaded by SUSTech on 2/2/2025 12:20:35 PM.

EP at each step into the spectral density of EP displacement (S_U), which reflects the EPO of the ion cores in real space.

(4) The velocity of the EPO (VEPO) at the ion cores $\Delta U_{ion}(t)$. Similar to the velocity of the ion cores, the difference between the EP of two adjacent time steps is defined as the velocity of the EP at the ion cores. By applying the PSD technique, the spectral density of VEPO ($S_{\Delta U}$) is obtained, which reflects the velocity of the EP value change at the ion cores.

The four signals of heavy and light atoms at four temperatures with a simulation time of 10 ps were analyzed using the PSD method. The distributions of S_D and S_U, S_V and $S_{\Delta U}$ of Ga and N atoms are very similar, as well as the frequency corresponding to the main peaks in GaN at 100 K, as shown in Fig. 5a–d. The same phenomenon was observed for heavy and light atoms at other temperatures, as shown in Fig. S3.† It can be concluded that the EPO of heavy and light atoms in diatomic semiconductors at different temperatures is caused by the lattice vibrations of heavy and light atoms, and the PSD method provides a clear physical picture to facilitate a better understanding of eqn (3). The non-uniformity of the peaks of lattice vibrations and EPO at specific frequencies may be attributed to the difference in the rate of distribution changes between the ion cores and electrons.

The concept of EPO at the finite atomic temperature is introduced. Lattice vibrations and EPO of heavy and light atoms intensify with increasing temperature. To verify this relationship in the diatomic semiconductors, the low and high temperatures were selected as 300 and 700 K, respectively, and the simulation time was 100 ps. The DEP and VEPO of the ion cores of heavy and light atoms were analyzed by using a fast Fourier transform (FFT), as shown in Fig. 5e and f and Fig. S4.†

The amplitude of DEP reflects the strength of EPO while the amplitude of VEPO reflects the rate of EPO change. As the temperature increases from 300 to 700 K, both the DEP amplitudes and VEPO amplitudes of the ion cores of Ga and N atoms in GaN rise. It is observable that blue signifies low-temperature areas and red signifies high-temperature areas. Across the 0–20 THz frequency range, the amplitudes of the predominantly red high-temperature zones consistently surpass those of the blue low-temperature zones. Similar results are observed in heavy and light atoms for AlN, ZnO, and SiC. This result indicates that the EPO intensity and the rate of EPO change in heavy and light atoms are elevated by increasing the temperature of the diatomic semiconductors. Thus, it is concluded that temperature exerts a driving effect on EPO.

3.5 Connection between EPO and electron thermal transfer

Previous studies have shown that the thermal conductivity of GaN exhibits a significant anisotropy between its in-plane and out-of-plane directions.[38–40] Similarly, regarding the studies on electronic properties, experiments indicate that the electron mobility of GaN also possesses anisotropy.[41–43] As the temperature rises from 300 to 700 K, within an electron concentration range of 10^{19} to 10^{21} cm^{-3}, the κ_e of GaN increases along the x and z axes at the same electron concentration, thus enhancing electronic thermal transport, as shown in Fig. 6a and b. Furthermore, at 300 and 700 K, with the increase in the concentration of electrons, the phenomenon that the κ_e along the z axes is greater than that along the x axes at the same electron concentration becomes more pronounced, indicating that the thermal transport conductivity of the electrons along the z axes is stronger compared to that along the x axes.

When the temperature is 700 K, the in-plane and out-of-plane κ_{ph} of GaN are 163 and 177 W m^{-1} K^{-1}, respectively, both of which have decreased compared to those at 300 K. With an increase in temperature from 300 to 700 K, the probability of thermal excitation of electrons and holes in the semiconductor increases, allowing electrons to transition from the valence band to the conduction band and become free electrons, resulting in an increase in the concentration of electrons.

By analyzing electron concentrations of 10^{19}, 10^{20}, and 10^{21} cm^{-3}, the proportion of κ_e to κ (the sum of κ_e and κ_{ph}) are determined. When the electron concentration reaches 10^{19} cm^{-3}, the contributions of in-plane and out-of-plane κ_e to the κ increase from 0.11% and 0.10% (at 300 K) to 0.21% and 0.20%

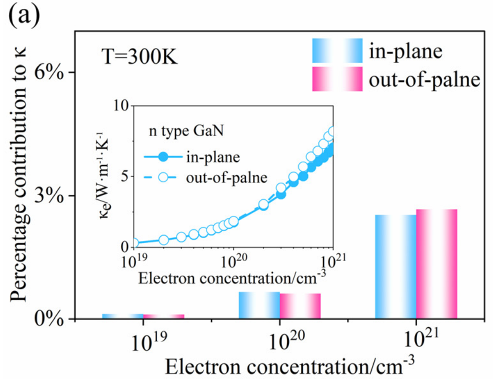

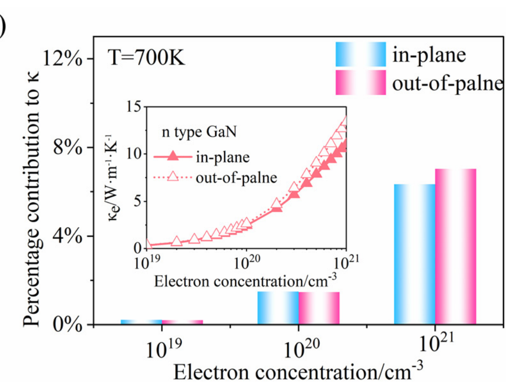

Fig. 6 Contribution of κ_e to the total thermal conductivity κ at (a) 300 and (b) 700 K. The inset shows κ_e as a function of electron concentration along different axes in n-type GaN at 300 and 700 K.

Published on 06 January 2025. Downloaded by SUSTech on 2/2/2025 12:20:35 PM.

(at 700 K), respectively. When the electron concentration reaches 10^{20} cm^{-3}, these contributions rise from 0.65% and 0.61% (at 300 K) to 1.49% and 1.47% (at 700 K), respectively. When the electron concentration reaches 10^{21} cm^{-3}, the contributions increase from 2.53% and 2.66% (at 300 K) to 6.33% and 7.02% (at 700 K), respectively. During this process, the temperature increase drives EPO, and the contribution of κ_e increases, while the contribution of κ_{ph} decreases. This provides insights into the understanding of electron heat transfer from the perspective of EPO.

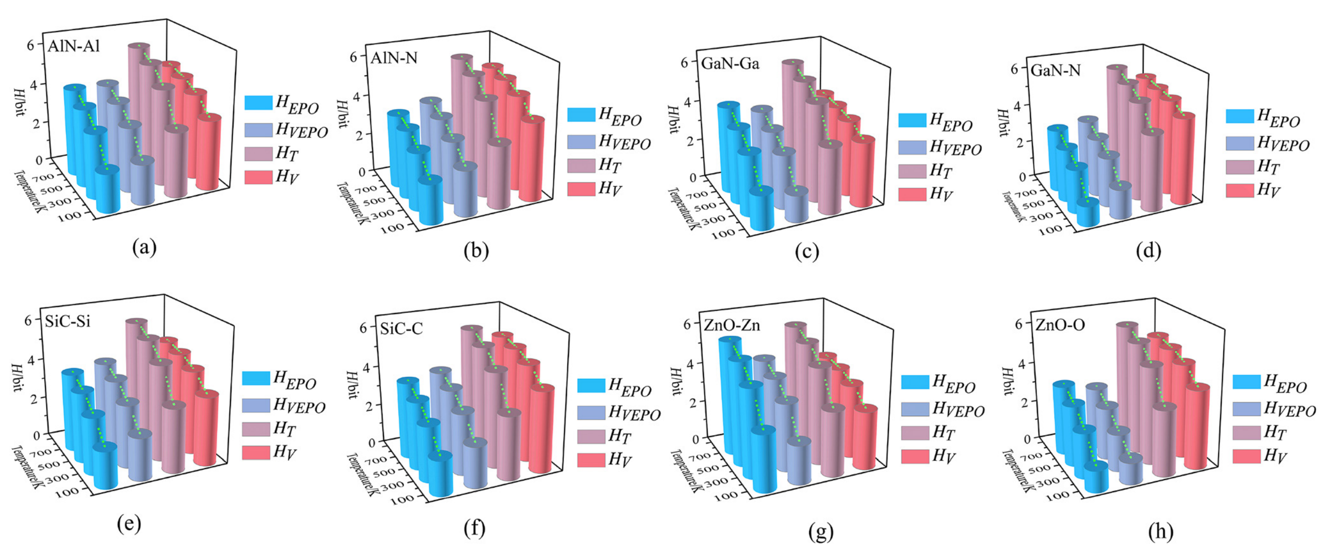

Fig. 7 H_{EPO}, H_{VEPO}, H_V, and H_T of (a) Al and (b) N, (c) Ga and (d) N, (e) Si and (f) C, (g) Zn and (h) O, at 100, 300, 500, and 700 K. The trend of entropy increase is represented by the curves.

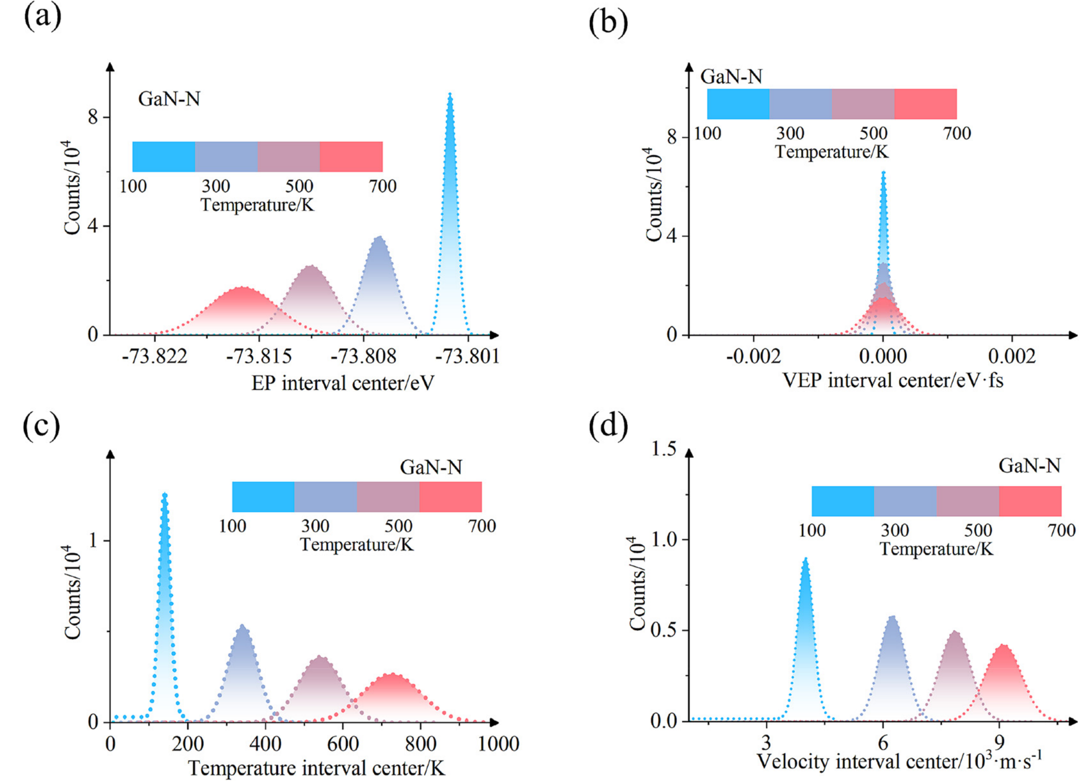

Fig. 8 Gaussian fitting of (a) EP, (b) VEP, (c) atomic temperature, and (d) atomic velocity distributions of N atoms in GaN, at 100, 300, 500, and 700 K.

This journal is © The Royal Society of Chemistry 2025

3.6 Uncertainties in atomic lattice vibrations and EPO

Entropy[44,45] as a function of a quantitative measure of uncertainty, and Shannon entropy[46–49] are commonly used. For a finite sequence of non-negative numbers, the Shannon entropy $H(p_i)$ of a probability vector p_i is defined as in eqn (9).[50,51] The unit of Shannon entropy is bit.

$$H(p_i) = -\sum_{i=1}^{n} p_i \log_2 p_i \quad \left(\sum_{i=1}^{n} p_i = 1,\ i = 1, 2, \ldots, n\right) \tag{9}$$

The entropy of the canonical ensemble also follows this form.[52] According to (eqn 9), the distributions of EPO, VEPO, temperature, and velocity of heavy and light atoms are partitioned according to the same interval length, and their respective frequency distributions correspond to p_i in the equation. Thus, the entropies of atomic EPO (H_{EPO}), atomic VEPO (H_{VEPO}), atomic temperature (H_T), and atomic velocity (H_V) are obtained. $H(p_i) = 0$ for $p_i = 0$. EPO, VEPO, atomic velocity, and atomic temperature distribution splitting intervals are 10^{-3} eV, 10^{-4} eV fs, 50 m s^{-1}, and 5 K, respectively.

It can be observed that the four entropies of Al and N, Ga and N, Si and C, Zn and O increase for the temperature from 100 to 700 K, as shown in Fig. 7. The trend of entropy increase is represented by the curves. The four entropies defined are also consistent with the principle of entropy increase.[51,53] For the four diatomic semiconductors, both heavy and light atoms conform to this result.

As the temperature increases from 100 to 700 K, the EP, VEPO, atomic velocity and atomic temperature distributions of N atoms in GaN go from a centralized distribution to a dispersed distribution, as shown in Fig. 8, the p_i on two sides of the distribution increase, and its H_{EPO}, H_{VEPO}, H_V, and H_T increase. Similarly, the increase in H_{EPO}, H_{VEPO}, H_V, and H_T values of heavy and light atoms in the other diatomic semiconductors is observed with increasing temperature, as shown in Fig. S6 and S7.†

4. Conclusions

In summary, the atomic temperatures and velocities of heavy and light atoms in AlN, GaN, InN, ZnO, and SiC are calculated separately at finite temperatures. Heat and kinetic energy transfer occur between heavy and light atoms. The lattice vibrations of Al and N, Ga and N, and In and N exhibit different phase differences at 300 K, it offers insights into understanding anharmonicity in semiconductor thermal conduction at finite temperatures. Phonon thermal conductivity in GaN and InN at 300 K is primarily derived from low-frequency acoustic phonons, which contribute to the in-plane thermal conductivity by accounting for 60% and 59%, respectively. In diatomic semiconductors, the EPO of atoms is caused by lattice vibrations at finite temperatures. The intensity and the rate of EPO changes in the atoms increase with increasing temperature. Temperature drives changes in the EP field of atoms in semiconductors, thereby affecting the thermal transport of electrons. Uncertainties in lattice vibrations and electrostatic potentials of atoms are described. The entropies of atomic EPO, atomic VEPO, atomic temperature, and atomic velocity are defined and the four entropies of the studied heavy and light atoms are in accordance with the principle of entropy increases as the temperature increases. This study not only broadens our understanding of lattice vibrations and EPO in different types of atoms within semiconductors but also lays the foundation for future studies on electron thermal transport in semiconductors.

Data availability

The data supporting the findings of this study are available from the corresponding author upon reasonable request.

Conflicts of interest

The authors declare no conflict of interest.

Acknowledgements

G. H. Tang thanks the support of the National Key Research and Development Program of China (Grant No. 2022YFC2204302), the National Natural Science Foundation of China (Grant No. 52130604), and the Shandong Provincial Natural Science Foundation (Grant No. ZR2023ZD18). S. Y. Yue thanks the support of the National Natural Science Foundation of China (GYKP022), and the Xi'an Jiaotong University Young Talent Program (LX6J0240001). Z. B. Gao thanks the support of the National Natural Science Foundation of China (No. 12104356). The work was carried out at the National Supercomputer Center in Tianjin, and the calculations were performed on Tianhe new generation supercomputer.

References

1 C. Tan, Z. Dong, Y. Li, H. Zhao, X. Huang, Z. C. Zhou, J. W. Jiang, Y. Z. Long, P. Jiang, T. Y. Zhang and B. Sun, *Nat. Commun.*, 2020, **11**, 3530.
2 W. Liu, Y. Liu, S. Zhong, J. Chen, Z. Li, C. Zhang, P. Jiang and X. Huang, *Small*, 2024, **20**, 2400115.
3 T. Gong, Y. Wu, L. Gao, L. Zhang, J. Li and T. Ming, *Energy*, 2019, **172**, 1211–1224.
4 W. Sun, R. Sui, G. Yuan, H. Zheng, Z. Zeng, P. Xie, L. Yuan, Z. Ren, F. Cai and Q. Zhang, *Mater. Today Phys.*, 2021, **18**, 100391.
5 Y. Qin, B. Qin, T. Hong, X. Zhang, D. Wang, D. Liu, Z. Y. Wang, L. Su, S. Wang, X. Gao, Z. H. Ge and L. D. Zhao, *Science*, 2024, **383**, 1204–1209.

Published on 06 January 2025. Downloaded by SUSTech on 2/2/2025 12:20:35 PM.

Published on 06 January 2025. Downloaded by SUSTech on 2/2/2025 12:20:35 PM.

6 P. Bai, Q. Zhang, H. Cui, Y. Bo, D. Zhang, W. He, Y. Chen and R. Ma, *Adv. Mater.*, 2023, **35**, 2209181.
7 Q. Jin, T. Guo, N. Perez, N. Yang, X. Jiang, K. Nielsch and H. Reith, *Nano-Micro Lett.*, 2024, **16**, 126.
8 C. Kittel, *Introduction to Solid States Physics*, John Wiley and Sons Inc, 2005.
9 Y. Pei, L. Chen, W. Jeon, Z. Liu and R. Chen, *Nat. Commun.*, 2023, **14**, 8242.
10 J. Zhou, H. D. Shin, K. Chen, B. Song, R. A. Duncan, Q. Xu, A. A. Maznev, K. A. Nelson and G. Chen, *Nat. Commun.*, 2020, **11**, 6040.
11 R. Woods-Robinson, Y. Han, H. Zhang, T. Ablekim, I. Khan, K. A. Persson and A. Zakutayev, *Chem. Rev.*, 2020, **120**, 4007–4055.
12 X. Yan, Q. Jin, Y. Jiang, T. Yao, X. Li, A. Tao, C. Gao, C. Chen, X. Ma and H. Ye, *ACS Appl. Mater. Interfaces*, 2022, **14**, 36875–36881.
13 J. Wu, *J. Appl. Phys.*, 2009, **106**, 011101.
14 S. Y. Yue, X. Zhang, S. Stackhouse, G. Qin, E. Di Napoli and M. Hu, *Phys. Rev. B.*, 2016, **94**, 075149.
15 S. Yue and M. Hu, *J. Appl. Phys.*, 2018, **125**, 045102.
16 H. M. Friedman, B. K. Agarwalla, O. Shein-Lumbroso, O. Tal and D. Segal, *Phys. Rev. B*, 2020, **101**, 195423.
17 H. Cui, L. Zhou, Y. Li and B. Kang, *Chaos, Solitons Fractals*, 2022, **155**, 111736.
18 D. S. Ageev, A. A. Bagrov and A. A. Iliasov, *Phys. Rev. B*, 2021, **103**, L100302.
19 G. Kresse and D. Joubert, *Phys. Rev. B:Condens. Matter Mater. Phys.*, 1999, **59**, 1758–1775.
20 P. E. Blochl, *Phys. Rev. B:Condens. Matter Mater. Phys.*, 1994, **50**, 17953–17979.
21 G. Kresse and J. Furthmuller, *Phys. Rev. B:Condens. Matter Mater. Phys.*, 1996, **54**, 11169–11186.
22 J. Hafner, *J. Comput. Chem.*, 2008, **29**, 2044–2078.
23 J. P. Perdew, K. Burke and M. Ernzerhof, *Phys. Rev. Lett.*, 1997, **78**, 1396–1396.
24 M. C. Payne, M. P. Teter, D. C. Allan, T. A. Arias and J. D. Joannopoulos, *Rev. Mod. Phys.*, 1992, **64**, 1045–1097.
25 G. J. Martyna, M. L. Klein and M. Tuckerman, *J. Chem. Phys.*, 1992, **97**, 2635–2643.
26 V. Wang, N. Xu, J. C. Liu, G. Tang and W. T. Geng, *Comput. Phys. Commun.*, 2021, **267**, 108033.
27 A. M. Ganose, J. Park, A. Faghaninia, R. Woods-Robinson, K. A. Persson and A. Jain, *Nat. Commun.*, 2021, **12**, 2222.
28 A. Togo and I. Tanaka, *Scr. Mater.*, 2015, **108**, 1–5.
29 W. Li, J. Carrete, N. A. Katcho and N. Mingo, *Comput. Phys. Commun.*, 2014, **185**, 1747–1758.
30 P. Rinke, M. Winkelnkemper, A. Qteish, D. Bimberg, J. Neugebauer and M. Scheffler, *Phys. Rev. B:Condens. Matter Mater. Phys.*, 2008, **77**, 075202.
31 C. Qi, L. Yu, X. Zhu, S. Li, K. Du, Z. Qin, G. Qin and Z. Xiong, *Phys. Chem. Chem. Phys.*, 2022, **24**, 21085–21093.
32 S. Mehta and K. Joshi, *Appl. Surf. Sci.*, 2022, **602**, 154150.
33 D. Wang, L. Zhang, D. Han, L. Niu, X. Zhong, X. Qu, L. Yang, J. Zhao and H. Li, *Phys. Chem. Chem. Phys.*, 2018, **20**, 26846–26852.
34 S. Li, L. Yu, C. Qi, K. Du, G. Qin and Z. Xiong, *Front. Mater.*, 2021, **8**, 725219.
35 L. C. Xu, R. Z. Wang, X. Yang and H. Yan, *J. Appl. Phys.*, 2011, **110**, 043528.
36 S. N. Girard, J. He, X. Zhou, D. Shoemaker, C. M. Jaworski, C. Uher, V. P. Dravid, J. P. Heremans and M. G. Kanatzidis, *J. Am. Chem. Soc.*, 2011, **133**, 16588–16597.
37 Z. Chen, X. Zhang and Y. Pei, *Adv. Mater.*, 2018, **30**, 1705617.
38 A. Chen, D. Wei, J. Xu, A. Li, H. Wang, Z. Qin and G. Qin, *J. Phys. Chem. Lett.*, 2023, **14**, 9746–9757.
39 B. Wei, Y. Li, W. Li, K. Wang, Q. Sun, X. Yang, D. L. Abernathy, Q. Gao, C. Li, J. Hong and Y. H. Lin, *Phys. Rev. B*, 2024, **109**, 155204.
40 J. Xue, F. Li, A. Fan, W. Ma and X. Zhang, *Int. J. Heat Mass Transfer*, 2024, **233**, 126049.
41 M. McLaurin, T. E. Mates, F. Wu and J. S. Speck, *J. Appl. Phys.*, 2006, **100**, 063707.
42 S. Jang, H. Kim, D. S. Kim, S. M. Hwang, J. Kim and K. H. Baik, *Appl. Phys. Lett.*, 2013, **103**, 162103.
43 Y. Lin, J. Wang, M. Pristovsek, Y. Honda and H. Amano, *J. Appl. Phys.*, 2023, **134**, 235701.
44 M. Aggarwal, *Eng. Appl. Artif. Intell.*, 2021, **104**, 104290.
45 A. Shavit and C. Gutfinger, *Thermodynamics: from concepts to applications*, CRC Press, 2008.
46 R. M. T. Madiona, D. L. J. Alexander, D. A. Winkler, B. W. Muir and P. J. Pigram, *Appl. Surf. Sci.*, 2019, **493**, 1067–1074.
47 B. Shiferaw, L. Downey and D. Crewther, *Neurosci. Biobehav. Rev.*, 2019, **96**, 353–366.
48 H. Zhang and Y. Deng, *Inf. Sci.*, 2021, **561**, 141–151.
49 Y. Xue and Y. Deng, *Chaos, Solitons Fractals*, 2022, **156**, 111835.
50 A. Srivastava and L. Kaur, *Int. J. Intell. Syst.*, 2019, **34**, 1248–1260.
51 T. Downarowicz, *Entropy in dynamical systems*, Cambridge University Press, 2011.
52 A. Svidzinsky, M. Kim, G. Agarwal and M. O. Scully, *New J. Phys.*, 2018, **20**, 013002.
53 W. Z. Zheng, Y. Liang and J. P. Huang, *Front. Phys.*, 2014, **9**, 128–135.

This journal is © The Royal Society of Chemistry 2025